



**HAL**  
open science

## Physical and electrochemical behaviors of AgX (X = S/I) in a GeS<sub>2</sub>–Sb<sub>2</sub>S<sub>3</sub> chalcogenide-glass matrix

Baochen Ma, Qing Jiao, Yeting Zhang, Xing Sun, Guoliang Yin, Xianghua Zhang, Hongli Ma, Xueyun Liu, Shixun Dai

► **To cite this version:**

Baochen Ma, Qing Jiao, Yeting Zhang, Xing Sun, Guoliang Yin, et al.. Physical and electrochemical behaviors of AgX (X = S/I) in a GeS<sub>2</sub>–Sb<sub>2</sub>S<sub>3</sub> chalcogenide-glass matrix. *Ceramics International*, 2020, 46 (5), pp.6544-6549. 10.1016/j.ceramint.2019.11.138 . hal-02493231

**HAL Id: hal-02493231**

**<https://univ-rennes.hal.science/hal-02493231>**

Submitted on 27 Feb 2020

**HAL** is a multi-disciplinary open access archive for the deposit and dissemination of scientific research documents, whether they are published or not. The documents may come from teaching and research institutions in France or abroad, or from public or private research centers.

L'archive ouverte pluridisciplinaire **HAL**, est destinée au dépôt et à la diffusion de documents scientifiques de niveau recherche, publiés ou non, émanant des établissements d'enseignement et de recherche français ou étrangers, des laboratoires publics ou privés.

## Physical and electrochemical behaviors of AgX (X = S/I) in a GeS<sub>2</sub>-Sb<sub>2</sub>S<sub>3</sub> chalcogenide-glass matrix

Baochen Ma<sup>1</sup>, Qing Jiao<sup>1\*</sup>, Yeting Zhang<sup>1</sup>, Xing Sun<sup>2</sup>, Guoliang Yin<sup>2</sup>, Xianghua Zhang<sup>3</sup>, Hongli Ma<sup>3</sup>, Xueyun Liu<sup>1</sup>, Shixun Dai<sup>1</sup>

<sup>1</sup> Laboratory of Infrared Material and Devices, Advanced Technology Research Institute, Ningbo University, Ningbo 315211, China

<sup>2</sup> Yunnan KIRO-CH Photonics Co., Ltd, No. 5 Hongwai Road, Economic and Technological Development Zone, Kunming, P.R. China

<sup>3</sup> Laboratory of Glasses and Ceramics, Institute of Chemical Science, UMR CNRS 6226, University of Rennes 1, Rennes, France

### ABSTRACT

Ion-conducting chalcogenide glasses of a AgX (X = S/I)-modified GeSbS system were triumphantly synthesized through the conventional techniques of melt quenching. The evolution of the physical and structural natures of these samples were examined through density and microhardness tests, DSC, and Raman scattering spectroscopy. The electric features of the bulk samples were studied by means of impedance spectroscopy. Room-temperature ionic conductivity dramatically increased by six orders of magnitude from  $7.68 \times 10^{-10}$  to  $3.54 \times 10^{-4}$  S/cm with increasing Ag<sup>+</sup> content. The blocking effect, a novel phenomenon caused by the presence of a small amount of I ions in the glass system, was also observed, and its corresponding mechanism was proposed. The blocking effect hindered a portion of the mobile carriers in the network. Another phenomenon, i.e., the saturation of Ag ions, resulted in a slow increase in ionic conductivity at high Ag<sup>+</sup> dopant concentrations. These results provide novel insights into structural evolution and electrochemical properties of metal-doped solid electrolytes.

**Keywords:** chalcogenide glass, electrochemical property, impedance spectroscopy, pre-exponential factor

### 1. Introduction

Metal-doped chalcogenide glasses (CG), a new sort of fast ionic conductors, are well known for their unique electrical and mechanical properties; thus, these glasses are potential candidate materials for next-generation high-performance electrolytes[1-3]. Chalcogenide glass

electrolytes are isotropic, possess grain-free boundaries, can be conveniently processed into various shapes, and have higher ionic conductivity and wider electrochemical window than their oxide counterparts[4, 5]. In contrast to traditional liquid electrolytes, solid electrolytes are environment-friendly materials devoid of safety issues, such as liquid leakage, fire hazards and explosion risk. However, the applications of solid electrolytes remain limited due to several key problems. One of the most important limitations to the use of these electrolytes is the difficulty in ensuring enhanced free carrier transport in the glass network. Glasses modified with charge carriers, such as  $\text{Li}^+$ ,  $\text{Na}^+$ , and  $\text{Ag}^+$ , exhibit superior ionic conductivity at room temperature[6-8]. Kawamoto et al. demonstrated that the ionic activity of ternary  $\text{GeS}-\text{GeS}_2-\text{Ag}_2\text{S}$  glass introduced with a half ratio of  $\text{Ag}_2\text{S}$  can reach  $3 \times 10^{-4}$  S/cm[9]. Saienga et al. showed that  $\text{GeS}_2-\text{Ga}_2\text{S}_3-\text{LiI}-\text{Li}_2\text{S}$  glasses doped with more than 35 mol% Li have an outstanding value of  $1.62 \times 10^{-3}$  S/cm[10]. Therefore, addition of a large amount of carrier solution in the network is the major key to enhancing ionic conductivity.

The ionic migration channel is another key factor for improving solid electrolyte performance. Lin et al. illustrated that the effective ion conductivity of the  $\text{GeSbS}-\text{AgI}$  glass system, which has the lowest value of  $E_a$  (0.07 eV) among other Ag-ion amorphous electrolytes, benefits from chain structure of ionic conductivity formed by  $[\text{SbSI}]$ . Kim et al. also found that the two-dimensional ionic channels in a  $\text{Na}_2\text{Se}-\text{Ga}_2\text{Se}_3-\text{GeSe}_2$  ternary system comprise  $[\text{Ge}_2\text{Se}_5]^{2-}$  anionic layers that are composed of  $[\text{GeSe}_4]^{4-}$  tetrahedra with three corner-shared neighboring tetrahedra units[11]. Na ions in such an anionic topology framework present high mobility and a long transport range through this layered phase. Therefore, inorganic materials characterized by charge carriers with high solubility and excellent ionic channels could be good alternative solid-state electrolytes in batteries.

Although samples with high ionic conductivity have been successfully prepared in previous studies, the change rule associated with several electrical parameters remains unclear. Thus, the applications of these samples in batteries are also limited. Moreover, the pre-exponential factor

$\sigma_0$ , a parameter highly responsive to the scale of carriers' migration, is a frequently controversial issue because of its irregular variation trend, and the low mechanical and thermal stability of chalcogenide solid-electrolyte cannot be ignored. Thus, further investigation and optimization of the physical and electrochemical properties of CG system are necessary.

In the present work, a ternary  $(1-x)(0.5\text{GeS}_2-0.5\text{Sb}_2\text{S}_3)-x\text{Ag}_2\text{S}$  ( $0.1 \leq x \leq 0.6$ ) glass system was explored for the first time. The base glass system exhibited an extensive glass-forming range for metal sulfides.  $\text{Ag}_2\text{S}$  dopant was introduced into the matrix until a crystalline phase appeared to obtain GeSbS glasses with improved stability and conductivity. AgI, a cubic crystal with excellent electrochemical property, was further introduced to optimize the ionic channels and conductivity. The AC impedance method was employed to track the electrical properties of the samples. The evolution of conductivity combined with structural changes was proposed. The results of this work can help elucidate ion transport and change rules of electrochemical parameters in metal-doped glass network.

## 2. Experimental

The raw materials used to synthesize glass included high-purity elemental Ge (5N), Sb (5N), and S (5N) and AgI (4N) and  $\text{Ag}_2\text{S}$  (3N) compounds. All glass samples were prepared via the traditional method of vacuum melt quenching. Each batch had an approximate weight of 10 g, and a specific stoichiometric ratio and was mixed in a quartz ampule with vacuum environment. The vacuum quartz ampule loaded with mixed ingredients was heated to 950 °C and melted in a rocking furnace for 10 h. Subsequently, the melts were quenched in water after cooling to 850 °C. The obtained samples were annealed for approximately 8 h to minimize internal stress and strain in the glass network. The resulting rod-like samples were made into discs with a thickness of 2.0 mm and a diameter of 10 mm. The surface of sample discs was polished for optical and electrical property measurements.

Densities were measured in conformity to the Archimedes principle. Microhardness was obtained from Vickers microindenter (Everone MH-3, China, 50g). The amorphous characteristic of the samples was determined

through X-ray diffraction (Bruker D2 Phaser at 30 kV, 10 mA, Cu  $K\alpha$ ) over the  $2\theta$  angle range of  $10^\circ$ – $70^\circ$ . The characteristic temperature of the samples was determined by a Q2000 workstation (TA, New Castle, USA,  $10^\circ\text{C}/\text{min}$ ) under a working atmosphere of inert gases. Raman scattering spectra (Renishaw In Via, Gloucestershire, UK, A YAG: Ar ion laser 785nm) were used to examine the structural evolution of the glass network. The polished discs were sputtered with Au to guarantee a good contact with the electrodes and form as a function of block electrode. Then, the as-prepared chalcogenide glass electrolytes were subjected to AC impedance measurements (Zahner IM6) over the range of 1 to  $1 \times 10^6$  Hz.

### 3. Results and discussion

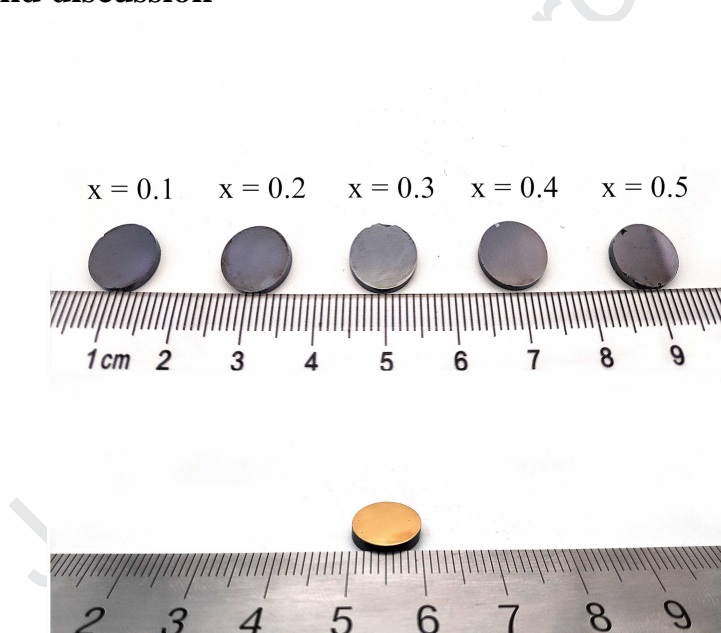


**Fig. 1.** Photos of the investigated  $(1-x)\text{GeSbS}-x\text{Ag}_2\text{S}$  ( $0.1 \leq x \leq 0.5$ ) glass samples in the form of discs with thicknesses of 2 mm.

Optically polished glass samples doped with 0.1–0.5  $\text{Ag}_2\text{S}$  content are shown in Fig. 1. All samples were almost opaque and difficult to distinguish on the basis of appearance. Unevenly distributed holes gradually appeared on the surfaces of glass rods when high concentrations of  $\text{Ag}^+$  were introduced into the matrix. This phenomenon can be ascribed to the existence of disconnected nonbridging S (NBS) bonds caused by  $\text{Ag}^+$  in the network. A previous work showed that the number of holes in the  $\text{Ag}_2\text{S}-\text{AgI}$  system is considerably less than that of  $\text{AgI}$  system with the same base glass component. This phenomenon

implies that mechanical stability has been optimized. The obtained samples were sputtered with Au, which was used as the block electrode for glass electrolytes.

### 3.1. XRD analysis

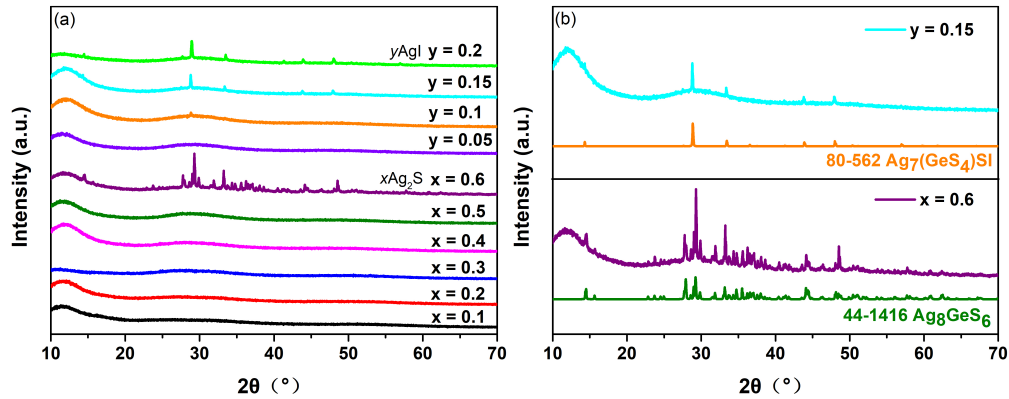


**Fig. 2.** (a) XRD patterns of as-prepared GeSbS–Ag<sub>2</sub>S and GeSbS–Ag<sub>2</sub>S–AgI samples; (b) Comparison of JCPDF Card Nos. 44-1416 Ag<sub>8</sub>GeS<sub>6</sub> and 80-562 Ag<sub>7</sub>(GeS<sub>4</sub>)SI with the XRD patterns of powder samples of  $x = 0.6$  and  $y = 0.15$ .

The powder XRD patterns of the  $(1-x)(0.5\text{GeS}_2-0.5\text{Sb}_2\text{S}_3)-x\text{Ag}_2\text{S}$  ( $0.1 \leq x \leq 0.6$ ) and  $(1-y)[0.5(0.5\text{GeS}_2-0.5\text{Sb}_2\text{S}_3)-0.5\text{Ag}_2\text{S}]-y\text{AgI}$  ( $0.05 \leq y \leq 0.2$ ) glass systems are presented in Fig. 2. Samples with  $x = 0.1-0.5$  and  $y = 0.05$  had an amorphous nature (Fig. 2[a]). An extensive crystalline phase appeared with further introduction of  $\text{Ag}^+$  at  $x = 0.6$  and  $y = 0.1-0.2$ . As shown in Fig. 2 (b), the consistency of Bragg peaks in the XRD pattern and JCPDF cards confirmed that precipitation of  $\text{Ag}_8\text{GeS}_6$  and  $\text{Ag}_7(\text{GeS}_2)\text{S}_3\text{I}$  is dominant crystalline phase in the glass matrix. This result indicated that large amounts of  $\text{Ag}^+$  are incorporated into the glass matrix, thereby increasing the carrier content in the network.

### 3.2. Physical and thermal behavior

**Table 1.** Relevant density, hardness and thermal parameters of all prepared inorganic materials.

Composition	Ag <sub>2</sub> S	AgI	$\rho$ ( $\pm 0.005$ g/cm <sup>3</sup> )	H <sub>v</sub> ( $\pm 3$ kg/mm <sup>2</sup> )	T <sub>g</sub> ( $\pm 2$ °C)
x = 0.1	0.1	0	3.978	186	240
x = 0.2	0.2	0	4.234	183	223
x = 0.3	0.3	0	4.528	178	216
x = 0.4	0.4	0	4.765	171	209
x = 0.5	0.5	0	5.119	169	194
x = 0.6	0.6	0	-	-	182
y = 0.05	0.475	0.05	5.084	158	191
y = 0.1	0.45	0.1	5.087	153	190
y = 0.15	0.425	0.15	5.149	143	188
y = 0.2	0.4	0.2	-	-	186

The specific physical information of all prepared samples is listed in Table 1. Density improved when the concentration of Ag<sub>2</sub>S was increased. The fluctuation observed with addition of AgI could be ascribed to the higher atomic mass of Ag<sub>2</sub>S compared with that of AgI[12]. Microhardness is usually related to the degree of network connectivity. Ag<sup>+</sup> itself is incorporated into the structure bonded with [–S]<sup>–</sup> and terminates amounts of structural chains. Therefore, the addition of Ag ions does not increase structural connectivity and, instead, continuously reduces sample hardness.

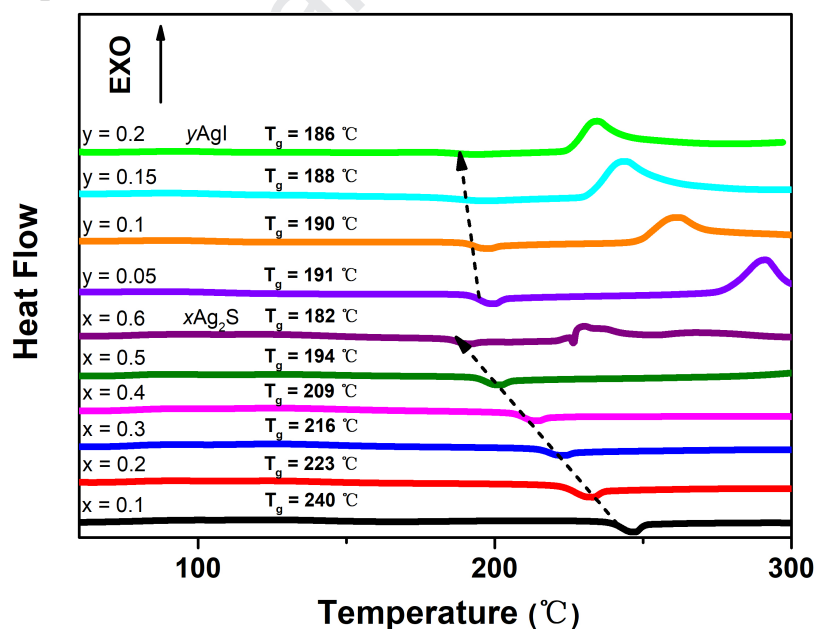


**Fig. 3.** Representative DSC curves of all samples heated at 10 °C/min under an inert atmosphere.

The thermal stability of Ag<sub>2</sub>S/AgI-singly doped and codoped samples on the basis of characterization temperature is illustrated in Fig. 3. The change in T<sub>g</sub> related to the bond strength of network linkages comprises

two stages in the current systems.  $T_g$  first decreased by 88 °C as the  $\text{Ag}_2\text{S}$  content increased from 0 to 0.6 ( $T_g = 270$  °C at  $x = 0$ ). Afterwards, the  $T_g$  remained stable at approximately 190 °C rather than changing drastically with continuous addition of  $\text{AgI}$  ( $0.05 \leq y \leq 0.2$ ). Addition of  $\text{Ag}^+$  as the network modifier may be responsible for the bond breakage of  $[\text{Sb}-\text{S}\dots\text{S}-\text{Sb}]$  and  $[\text{Ge}-\text{S}\dots\text{S}-\text{Ge}]$  chains[13]. Severe reductions in  $T_g$  are frequently accompanied by reductions in the interconnections of units, which means the interconnected S bonds are largely destroyed by  $\text{Ag}^+$  at high concentrations of  $\text{Ag}^+$ . Thus, introduction of  $\text{I}^-$  has negligible effect on  $T_g$  despite the role of  $\text{I}^-$  as a terminator. This finding seems incompatible with the empirical rule of dramatic reductions in  $T_g$  by  $\text{AgI}$ , which will be more instructive in the following Raman analysis.

### 3.3. Raman spectroscopy

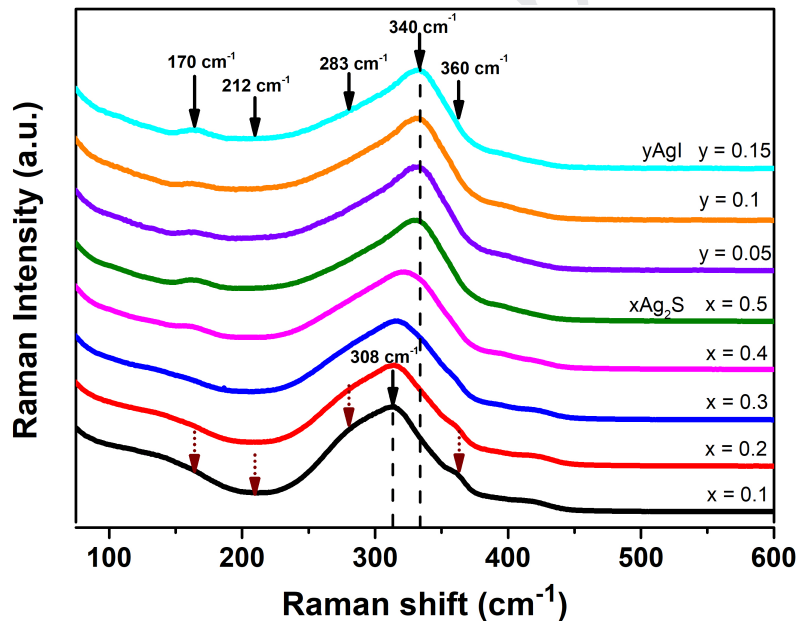


**Fig. 4.** Raman scattering spectra of  $(1-x)\text{GeSbS}-x\text{Ag}_2\text{S}$  ( $x = 0.1-0.5$ ) and  $(1-y)(\text{GeSbS}-\text{Ag}_2\text{S})-y\text{AgI}$  ( $y = 0.05-0.15$ ) bulk samples.

As-prepared samples were subjected to Raman spectroscopy to explore devitrification and thermal behaviors with structural correlations. The most intense peak near 283 and 308  $\text{cm}^{-1}$  could be ascribed to the asymmetric stretching vibrations of  $[\text{SbS}_{3/2}]$  pyramids, while those at 340  $\text{cm}^{-1}$  were attributed to corner-sharing (CS)  $[\text{GeS}_{4/2}]$  tetrahedra[14]. The decreased band near 360  $\text{cm}^{-1}$  can be credited to the symmetric stretching mode of edge-shared (ES)  $[\text{GeS}_{4/2}]$  tetrahedra. The increasing broad bands at 170 and 212  $\text{cm}^{-1}$  were attributed to  $[\text{S}_2\text{Sb}-\text{SbS}_2]$  and  $[\text{Ag}-\text{S}]$

units, respectively[13, 15]. The most intense peak shifts from  $308\text{ cm}^{-1}$  ( $x = 0.1$ ) to  $340\text{ cm}^{-1}$  at ( $x = 0.5$ ) could be attributed to the influence of the added  $\text{Ag}_2\text{S}$  on network bonding.

Ge is usually inclined to form CS tetrahedra ( $340\text{ cm}^{-1}$ ) than ES tetrahedra ( $360\text{ cm}^{-1}$ ) in the current matrix[16]. Thus, ES  $[\text{GeS}_{4/2}]$  units were easily transformed into CS  $[\text{GeS}_{4/2}]$  as  $\text{Ag}_2\text{S}$  content increased.  $\text{Ag}^+$  tended to degrade the bonding of Sb–S in  $[\text{S}_2\text{Sb–S}\dots\text{S–SbS}_2]$  units into homopolar  $[\text{S}_2\text{Sb–SbS}_2]$  units. Hence, the slight reduction in peaks at  $283$  and  $308\text{ cm}^{-1}$  at  $0.1 \leq x \leq 0.3$  confirm that  $\text{Ag}^+$  cleave the Sb–S bond ( $260\text{ kJ/mol}$ ) rather than Ge–S bond ( $265\text{ kJ/mol}$ ). At this stage,  $\text{Ag}^+$  breaks the bridging S (BS) by acting as a modifier in the network. This phenomenon causes a drastic reduction in  $T_g$ . At  $0.4 \leq x \leq 0.5$ , the homopolar bonds of Sb–Sb formed vibrations at  $170\text{ cm}^{-1}$ , which implies that clustering of  $\text{Ag}^+$  around Sb limits the formation of  $[\text{Sb–S–Sb}]$ . The drastic shift in the peak at  $308\text{ cm}^{-1}$  to  $340\text{ cm}^{-1}$  confirms that interconnected  $[\text{S}_2\text{Sb–S}\dots\text{S–SbS}_2]$  units are depleted and CS  $[\text{GeS}_{4/2}]$  units begin to form at the expense of ES  $[\text{GeS}_{4/2}]$  units. Therefore, samples with high  $T_g$  derive more benefit from ES  $[\text{GeS}_{4/2}]$  units than form CS  $[\text{GeS}_{4/2}]$  units, and  $T_g$  continues to decrease. XRD revealed that the crystalline phase  $\text{Ag}_8\text{GeS}_6$  appears at  $x = 0.6$ . This phase can be easily ascribed to the accumulation of excess  $\text{Ag}_2\text{S}$  dopant around CS  $[\text{GeS}_{4/2}]$  units. As a result,  $[\text{GeS}_{4/2}]$  coordinated with four  $\text{Ag}_2\text{S}$  units devitrified into  $\text{Ag}_8\text{GeS}_6$  ( $\text{GeS}_2 \cdot 4\text{Ag}_2\text{S}$ ) at the quenching stage. Similarly, large amount of crystalline phase  $\text{Ag}_7(\text{GeS}_2)\text{S}_3\text{I}$  precipitated at  $y = 0.15$  because of  $\text{AgI}$  saturation around CS  $[\text{GeS}_{4/2}]$  tetrahedra. The negligible effect of I, which acts as a glassy network terminator, on  $T_g$  can be attributed to the enhanced network stability induced by abundant S ions. In other words, addition of  $\text{Ag}_2\text{S}$  instead of  $\text{AgI}$  as the first dopant prevents the generation of fragmented structures, such as  $[\text{GeI}_4]$  or  $[\text{SbI}_3]$ . The substituted S ions could still form a chain structure with other cations upon introduction of  $\text{AgI}$  into the matrix. Therefore, network stability was optimized, and  $T_g$  was stable at  $190\text{ }^\circ\text{C}$ . These results are in good accordance with the devitrification and thermal behavior of our samples.

### 3.4. Ionic conductivity

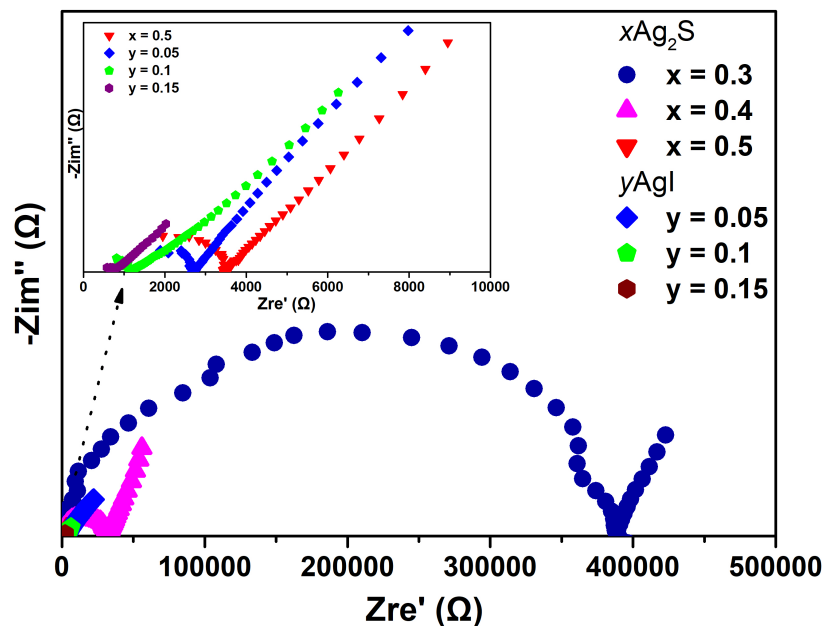


**Fig. 5.** Representative Nyquist plot of  $(1-x)GeSbS-xAg_2S$  ( $x = 0.3, 0.4, 0.5$ ) and  $(1-y)(GeSbS-Ag_2S)-yAgI$  ( $y = 0.05, 0.1, 0.15$ ) bulk samples. The inset presents a magnified image of the marked area.

A typical impedance test was performed to explore the electrochemical properties of the system. The results are shown in Fig. 5, and a magnified diagram of the high-frequency area is shown in the inset of this figure. The plot was composed of  $Zre'$  and  $-Zim''$ , which respectively represent the real and imaginary parts of impedance. A semicircle (or its part) was present in the region of high-frequency current, and a tail was observed in the region of low-frequency current. The intrinsic impedance of the bulk material was characterized by the radius of a single arc. Electrode polarization was responsible for the tail, which implies that the transport mechanism of ionic migration is dominated in the glass network. The real resistance existed in bulk samples was able to be evaluated from the junction of the impedance curve with the x-axis. In this work, the single semicircles all presented the expected trend, wherein the diameter of the arc decreased and the intersection moved to a low  $Zre'$  with increasing  $Ag_2S$  or  $AgI$  content. This phenomenon shows that most of the  $Ag^+$  acts as network modifiers instead of glass formers. Moreover, these ions can move through the ionic channels back and forth under the electrical field. Such behavior is ascribed to the reduced resistance of the bulk samples.

The ionic conductivity of samples was deduced from the equation  $\sigma = D/(S \cdot R)$ , where  $D$  stands for the thickness of discs, and  $S$  is the area of

sample sputtered with Au. In theory, metal-doped CG materials frequently obeys the Arrhenius Law, which is expressed as  $\sigma = \sigma_0/T \exp(-E_a/kT)$ . The Arrhenius equation is usually transformed into a simpler form  $\ln\sigma T = \ln\sigma_0 - E_a/kT$  to improve comprehensibility, where  $\sigma_0$  represents the pre-exponential factor of electrochemical reaction,  $E_a$  is the activation energy of ionic migration, and  $k$  stands for the Boltzmann constant[17]. Thus,  $\sigma_0$  and  $E_a$  can easily be deduced from the linear regression[7]. The Arrhenius plots for bulk samples within the range of characteristic temperature are presented in Fig. 6, and the results in the case of room-temperature  $\sigma_{303k}$  and  $E_a$  are shown in Table 2.

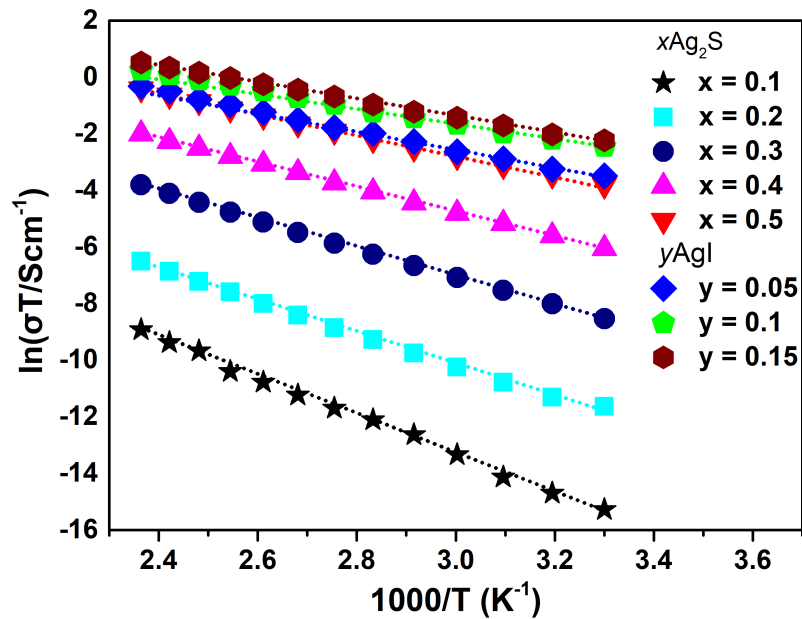


**Fig. 6.** Arrhenius behavior plots for bulk samples. The linear fittings of  $\ln(\sigma T)$  are displayed as a function of  $1000/T$ . Open symbols represent experimental values.

**Table 2.** Dependence of conductivity  $\log\sigma_{303K}$ , activation energy  $E_a$  and pre-exponential factor  $\sigma_0$  on Ag mole percentage.

Composition	Ag(mol%)	$\log\sigma_{303K}$ (S/cm)	$E_a$ (eV)	$\sigma_0$ (Scm <sup>-1</sup> K)
x = 0.1	5.12%	-9.11	0.58	1199.90
x = 0.2	10.52%	-7.53	0.47	820.57
x = 0.3	16.21%	-6.18	0.43	3165.29
x = 0.4	22.22%	-5.10	0.37	3677.54
x = 0.5	28.57%	-4.13	0.31	3364.02
y = 0.05	29.19%	-3.99	0.29	1096.63
y = 0.1	29.85%	-3.54	0.23	1339.43
y = 0.15	30.53%	-3.44	0.24	2038.56

The linear dependence of  $\ln\sigma T$  on  $1000/T$ , which can be ascribed to thermally activated mobility of  $Ag^+$ , was calculated, and the results are

given in Fig. 6. The ionic conductivity of the investigated bulk samples noticeably changed over the composition range and improved by six orders of magnitude from  $7.68 \times 10^{-10}$  S/cm to  $3.54 \times 10^{-4}$  S/cm at room temperature. The related  $E_a$  decreased from 0.58 eV (5.12 mol% Ag) to 0.24 eV (30.53 mol% Ag) with increasing dopant  $\text{Ag}^+$  concentration. By contrast, the pre-exponential factor  $\sigma_0$  rose from 1199.90  $\text{Scm}^{-1}\text{K}$  to 3364.02  $\text{Scm}^{-1}\text{K}$ . The pre-exponential factor  $\sigma_0$  is supposed to follow a proportional trend with increasing availability of mobile charge carriers in the network[18]. With further introduction of AgI, however,  $\sigma_0$  first suddenly dropped and then linearly increased. This sudden drop contradicts empirical findings and may be related to the  $\Gamma^-$ -induced structural motif of  $[\text{GeS}_{1.5}\text{I}]$  or  $[\text{SbSI}]$ .  $\Gamma^-$  bonded with Ge or Sb hinders the mobility of some  $\text{Ag}^+$ , which could cause  $\sigma_0$  to decrease. Then, a blocking effect was induced during  $\text{Ag}^+$  migration owing to the considerably larger radius of  $\Gamma^-$  (2.16 Å) compared with that of  $\text{Ag}^+$  (0.67 Å). This blocking effect was gradually weakened because of channel opening by  $\Gamma^-$  when the AgI content was increased. This result can be deduced from the slight increase in  $\sigma_{303\text{K}}$  and decrease in  $E_a$  between  $x = 0.5$  and  $y = 0.05$ . The slight increase in  $\sigma_{303\text{K}}$  implies that a reduced number of new  $\text{Ag}^+$  participates in migration and that the overall percentage of carriers has decreased. The negligible decrease in  $E_a$  illustrates that some of the  $\Gamma^-$  has negative effects on the ionic channels and, therefore, impedes ion migration. Thus, it is worthwhile to note that the pre-exponential factor is proportional to the scale of carrier's migration, but it is not necessarily inverse proportional to the activation energy in the current work.

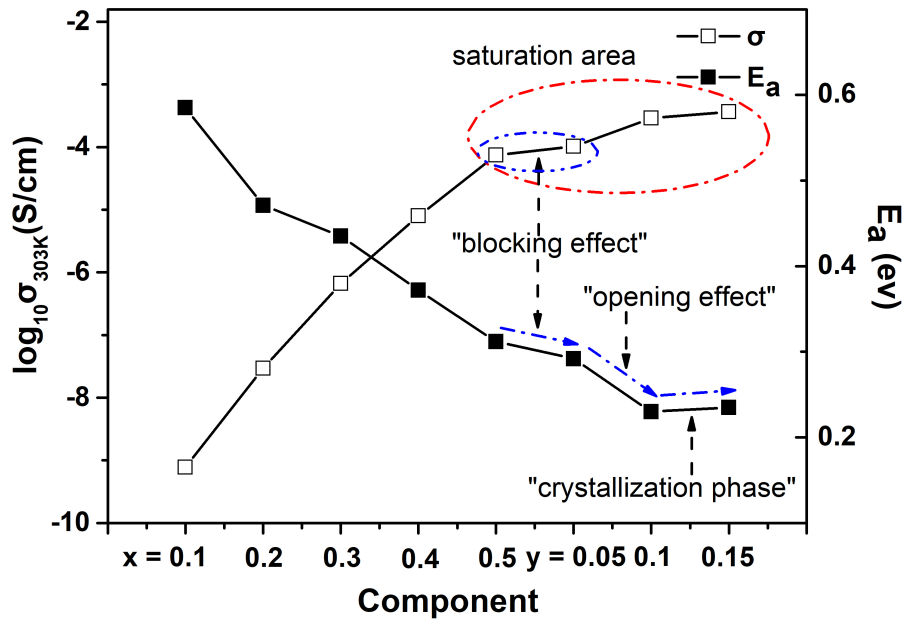


**Fig. 7.** Logarithmic form of conductance at 30 °C and activation energy  $E_a$  as a function of the composition of the studied samples.

The evolution of  $\log\sigma_{303K}$  and  $E_a$  with sample compositions of  $0.1 \leq x \leq 0.5$  and  $0.05 \leq y \leq 0.15$  is illustrated in Fig. 7. A linear increase and decrease in  $\log\sigma_{303K}$  and  $E_a$  over the range of  $0.1 \leq x \leq 0.5$  were respectively observed.  $Ag^+$  in the network was first randomly arranged and disordered before assembling and spreading all over the network. The network structure subsequently began to transform into  $[S_2Sb-SbS_2]$  and CS  $[GeS_{4/2}]$  units. With further addition of AgI into the matrix, an interesting phase with a slight change in ionic conductivity gradually develop. A large body of experimental evidence has shown that the electrical property of glass doped with AgI is better than that of glass with  $Ag_2S$  because the glassy framework doped with AgI provides an open and loose network environment that facilitates  $Ag^+$  conduction through the matrix[19-23]. In this work, however, the ionic conductivity of codoped samples did not significantly increase compared with that of  $Ag_2S$  single-doped samples. The saturation area of  $Ag^+$  (marked by dashed circle) was likely present in this situation. It should be noted that the related Raman band located in  $212\text{ cm}^{-1}$  which belongs to Ag-S vibrations did not drastically change when  $y = 0.05-0.15$ . This result indicates that  $Ag^+$  prefers to cluster in crystalline phases instead of acting as free carriers. Thus, devitrification of the metal crystalline phase was induced by excess  $Ag^+$  in the network. The obvious reduction in  $E_a$  at

$0.05 \leq y \leq 0.1$  without a considerable increase in  $\sigma_{303K}$  provides further evidence of the saturation phase. The number of  $\text{Ag}^+$  acting as free carriers nearly reached saturation and changed negligibly even when ionic channels are improved by  $\Gamma$ . This saturation area decelerated with increasing ionic conductivity. The blocking effect (marked by the arrow in the  $E_a$  curve and blue dashed circle in the  $\sigma$  curve) had a negative impact on  $E_a$  and then transformed into the opening effect with greater decreases of  $E_a$ . Finally, an increasing trend was observed in  $E_a$  because of extra grain boundary resistance caused by crystallization phase in the ionic channels. The densely packed grain boundaries produced additional obstruction to ion migration. Therefore, ionic conductivity increased linearly when only  $\text{Ag}_2\text{S}$  was introduced and slowly increased in the saturation area.

#### 4. Conclusion

In this work, samples of  $(1-x)\text{GeSbS}-x\text{Ag}_2\text{S}$  and  $(1-y)(\text{GeSbS}-\text{Ag}_2\text{S})-y\text{AgI}$  glass systems were successfully prepared, and the physical and electrochemical behaviors of the obtained systems were investigated. The thermal and mechanical performance of the samples was optimal at  $188\text{ }^\circ\text{C}$  and  $143\text{ kg/mm}^2$ . A remarkable  $\text{Ag}^+$  conductivity of  $3.54 \times 10^{-4}\text{ S/cm}$  and favorable  $E_a$  of  $0.24\text{ eV}$  were obtained with the optimal composition of  $y = 0.15$ . A novel blocking effect caused by a small amount of  $\Gamma$  occurred at  $y = 0.05$ , at which point the saturation phase of  $\text{Ag}^+$  carriers began to appear. Analyses revealed that the pre-exponential factor  $\sigma_0$  was proportional to the carrier migration rate. The  $\text{GeSbS}-\text{Ag}_2\text{S}-\text{AgI}$  system was characterized by optimized thermodynamic stability and rapid  $\text{Ag}^+$  conduction. Thus, this system provides new and exciting opportunities for developing a novel class of amorphous materials with applications in solid electrolytes.

#### Acknowledgement

This work was financially supported by National Natural Science Foundation of China (Grant no. 51972176, 61605093 and 51702172), Natural Science Foundation of Ningbo City (No. 2018A610140), Science Research Fund Project of Ningbo University (Grant Nos. XYL18015) and sponsored by K. C. Wong Magna Fund in Ningbo University.

Journal Pre-proof

## Reference

- [1] M. Bokova, A. Paraskiva, M. Kassem, I. Alekseev, E. Bychkov,  $\text{Ti}_2\text{S-GeS-GeS}_2$  system: Glass formation, macroscopic properties, and charge transport, *Journal of Alloys and Compounds* 777 (2019) 902-914. <http://doi.org/10.1016/j.jallcom.2018.10.375>.
- [2] D.S. Patil, M. Konale, S. Cozic, L. Calvez, V. Zima, T. Wagner, J.S. McCloy, D. Le Coq, Percolation behavior of Ag in  $\text{Ge}_{16}\text{Sb}_{12}\text{Se}_{72}$  glassy matrix and its impact on corresponding ionic conductivity, *Journal of Alloys and Compounds* 782 (2019) 375-383. <http://doi.org/10.1016/j.jallcom.2018.12.140>.
- [3] R. Tang, Z.-H. Zheng, Z.-H. Su, X.-J. Li, Y.-D. Wei, X.-H. Zhang, Y.-Q. Fu, J.-T. Luo, P. Fan, G.-X. Liang, Highly efficient and stable planar heterojunction solar cell based on sputtered and post-selenized  $\text{Sb}_2\text{Se}_3$  thin film, *Nano Energy* 64 (2019). <http://doi.org/10.1016/j.nanoen.2019.103929>.
- [4] W. Yao, S. Martin, Ionic conductivity of glasses in the  $\text{MI}+\text{M}_2\text{S}+(0.1\text{Ga}_2\text{S}_3+0.9\text{GeS}_2)$  system (M=Li, Na, K and Cs), *Solid State Ionics* 178(33-34) (2008) 1777-1784. <http://doi.org/10.1016/j.ssi.2007.10.011>.
- [5] C. Lin, E. Zhu, J. Wang, X. Zhao, F. Chen, S. Dai, Fast Ag-ion-conducting  $\text{GeS}_2\text{-Sb}_2\text{S}_3\text{-AgI}$  glassy electrolytes with exceptionally low activation energy, *The Journal of Physical Chemistry C* 122(3) (2018) 1486-1491. <http://doi.org/10.1021/acs.jpcc.7b10630>.
- [6] Y. Liu, D. Le Coq, J. Ren, L. Hu, G. Chen, Effects of Ag addition on properties and structure of  $\text{Ge-Ga-Se-AgI}$  chalcogenide glasses, *Journal of Non-Crystalline Solids* 432 (2016) 232-236. <http://doi.org/10.1016/j.jnoncrysol.2015.10.015>.
- [7] J. Ren, Q. Yan, T. Wagner, V. Zima, M. Frumar, B. Frumarova, G. Chen, Conductivity study on  $\text{GeS}_2\text{-Ga}_2\text{S}_3\text{-AgI-Ag}$  chalcogenide glasses, *Journal of Applied Physics* 114(2) (2013) 023701. <http://doi.org/10.1063/1.4813139>.
- [8] S. Cui, D. Le Coq, C. Boussard-Plédel, B. Bureau, Electrical and optical investigations in  $\text{Te-Ge-Ag}$  and  $\text{Te-Ge-AgI}$  chalcogenide glasses, *Journal of Alloys and Compounds* 639 (2015) 173-179. <http://doi.org/10.1016/j.jallcom.2015.03.138>.
- [9] Y. Kawamoto, N. Nagura, S. Tsuchihashi, ChemInform Abstract: DC CONDUCTIVITY OF  $\text{GE-S-AG}$  AND  $\text{AS-S-AG}$  GLASSES, *Chemischer Informationsdienst* 57(11) (2010) 489-491. <http://doi.org/10.1111/j.1151-2916.1974.tb11399.x>.
- [10] J. Saienga, S.W. Martin, The comparative structure, properties, and ionic conductivity of  $\text{LiI+Li}_2\text{S+GeS}_2$  glasses doped with  $\text{Ga}_2\text{S}_3$  and  $\text{La}_2\text{S}_3$ , *Journal of Non-Crystalline Solids* 354(14) (2008) 1475-1486. <http://doi.org/10.1016/j.jnoncrysol.2007.08.058>.
- [11] S.K. Kim, A. Mao, S. Sen, S. Kim, Fast Na-ion conduction in a chalcogenide glass-ceramic in the ternary system  $\text{Na}_2\text{Se-Ga}_2\text{Se}_3\text{-GeSe}_2$ , *Chemistry of Materials* 26(19) (2014) 5695-5699. <http://doi.org/10.1021/cm502542p>.

- [12] B. Ma, Q. Jiao, Y. Zhang, X. Sun, G. Yin, X. Zhang, H. Ma, X. Liu, S. Dai, Optimization of glass properties by substituting AgI with Ag<sub>2</sub>S in chalcogenide system, *Ceramics International* (2019). <http://doi.org/10.1016/j.ceramint.2019.07.305>.
- [13] M. Fraenkl, B. Frumarova, V. Podzemna, S. Slang, L. Benes, M. Vlcek, T. Wagner, How silver influences the structure and physical properties of chalcogenide glass (GeS<sub>2</sub>)<sub>50</sub>(Sb<sub>2</sub>S<sub>3</sub>)<sub>50</sub>, *Journal of Non-Crystalline Solids* 499 (2018) 412-419. <http://doi.org/10.1016/j.jnoncrysol.2018.07.046>.
- [14] H.-T. Guo, M.-J. Zhang, Y.-T. Xu, X.-S. Xiao, Z.-Y. Yang, Structural evolution study of additions of Sb<sub>2</sub>S<sub>3</sub> and CdS into GeS<sub>2</sub> chalcogenide glass by Raman spectroscopy, *Chinese Physics B* 26(10) (2017). <http://doi.org/10.1088/1674-1056/26/10/104208>.
- [15] M. Zhang, Z. Yang, L. Li, Y. Wang, J. Qiu, A. Yang, H. Tao, D. Tang, The effects of germanium addition on properties of Ga-Sb-S chalcogenide glasses, *Journal of Non-Crystalline Solids* 452 (2016) 114-118. <http://doi.org/10.1016/j.jnoncrysol.2016.08.023>.
- [16] C. Lin, Z. Li, L. Ying, Y. Xu, P. Zhang, S. Dai, T. Xu, Q. Nie, Network Structure in GeS<sub>2</sub>-Sb<sub>2</sub>S<sub>3</sub> Chalcogenide Glasses: Raman Spectroscopy and Phase Transformation Study, *The Journal of Physical Chemistry C* 116(9) (2012) 5862-5867. <http://doi.org/10.1021/jp208614j>.
- [17] PIARRISTEGUY, C. Garrido, M. J., UREFIA, A. M., FONTANA, A.J.J.o.N.-C. Solids, Conductivity percolation transition of Ag<sub>x</sub>(Ge<sub>0.25</sub>Se<sub>0.75</sub>)<sub>100-x</sub> glasses, 353(32-40) (2007) 3314-3317. <http://doi.org/10.1016/j.jnoncrysol.2007.05.078>.
- [18] M. Urena, A. Piarristeguy, M. Fontana, B. Arcondo, Ionic conductivity (Ag) in AgGeSe glasses, *Solid State Ionics* 176(5-6) (2005) 505-512. <http://doi.org/10.1016/j.ssi.2004.09.008>.
- [19] D. Fasquelle, J.-C. Carru, C. Renard, Electrical characterizations of silver chalcogenide glasses, *Journal of Non-Crystalline Solids* 353(11-12) (2007) 1120-1125. <http://doi.org/10.1016/j.jnoncrysol.2006.12.024>.
- [20] N. Chbani, A. Ferhat, A.M. Loireau-Lozac'H, J. Dugué, Electrical conductivity of Ag<sub>2</sub>S-Ga<sub>2</sub>S<sub>3</sub>-GeS<sub>2</sub> glasses, *Journal of Non-Crystalline Solids* 231(3) (1998) 251-256. [http://doi.org/10.1016/S0022-3093\(98\)00410-4](http://doi.org/10.1016/S0022-3093(98)00410-4).
- [21] G. Tang, C. Liu, L. Luo, W. Chen, Thermal properties, microstructure, and conductivity of new glasses based on the GeSe<sub>2</sub>-Ga<sub>2</sub>Se<sub>3</sub>-AgI system, *Journal of the American Ceramic Society* 91(12) (2008) 4171-4174. <http://doi.org/10.1111/j.1551-2916.2008.02816.x>.
- [22] S. Stehlik, V. Zima, T. Wagner, J. Ren, M. Frumar, Conductivity and permittivity study on silver and silver halide doped GeS<sub>2</sub>-Ga<sub>2</sub>S<sub>3</sub> glassy system, *Solid State Ionics* 179(33-34) (2008) 1867-1875. <http://doi.org/10.1016/j.ssi.2008.05.001>.
- [23] Z. Li, C. Lin, G. Qu, L. Calvez, S. Dai, X. Zhang, T. Xu, Q. Nie, Formation and

properties of chalcogenide glasses based on  $\text{GeS}_2\text{-Sb}_2\text{S}_3\text{-AgI}$  system, Materials Letters 132 (2014) 203-205. <http://doi.org/10.1016/j.matlet.2014.06.083>.

Journal Pre-proof

**Declaration of interests**

The authors declare that they have no known competing financial interests or personal relationships that could have appeared to influence the work reported in this paper.

The authors declare the following financial interests/personal relationships which may be considered as potential competing interests: